IEEE Access
Multidisciplinary | Rapid Review | Open Access Journal

Received October 31, 2018, accepted November 17, 2018, date of publication November 22, 2018,
date of current version December 27, 2018.

Digital Object Identifier 10.1109/ACCESS.2018.2882767

Accelerated Life Test for Reliability Evaluation of Pneumatic Cylinders

JUAN CHEN[1,2], ENRICO ZIO[2,3], (Senior Member, IEEE), JIA LI[4], ZHIGUO ZENG[2], AND CHONG BU[5]

[1]School of Mechanical Engineering and Automation, Beihang University, Beijing 100191, China
[2]Chair on Systems Science and the Energy Challenge, Fondation Electricité de France, Laboratoire Genie Industriel, CentraleSupélec, Université Paris Saclay, 91190 Gif-sur-Yvette, France
[3]Energy Department, Politecnico di Milano, 20156 Milan, Italy
[4]Siemens PLM Software, SIEMENS company, Beijing 100191, China
[5]School of Mechanical Electronic and Information Engineering, China University of Mining and Technology, Beijing 100083, China

Corresponding author: Zhiguo Zeng (zhiguo.zeng@centralesupelec.fr)

This work was supported by the China Scholarship Council under Grant 201706025028.

ABSTRACT Pneumatic cylinders are intended to be designed for high reliability and long lifetimes. Evaluating such designs through conventional life tests is difficult as the affordable test time is too short to generate a meaningful amount of failure data. In this paper, we design and implement an accelerated life test (ALT) for evaluating the reliability of pneumatic cylinders. From a detailed analysis of failed samples from field operation, the major failure mechanisms that affect the reliability of pneumatic cylinders are identified, e.g., wear and tear of sealing rings. For these failure mechanisms, temperature and frequency are found out to be the significant stresses of the pneumatic cylinders. A two-factor-four-level full-factor design of ALT is, then, performed to set up an ALT plan for the pneumatic cylinders. A total number of 95 samples are tested according to the ALT plan, and a mixed Arrhenius-inverse-power-law model is used to fit the test data and predict the reliability under normal operation conditions. In addition, a normal stress test of eight samples is performed to validate the reliability predicted by the ALT. The results show that using the proposed ALT, the reliability of the pneumatic cylinder can be predicted with satisfactory accuracy. It is also shown that the designed ALT plan requires only 38.77% of the testing effort of other conventional life tests.

INDEX TERMS Accelerated life test, data analysis, failure mechanisms, pneumatic cylinders, reliability.

I. INTRODUCTION

Pneumatic cylinders (sometimes also called air cylinders or actuators) are mechanical devices that use compressed air to produce force to drive reciprocating linear motions [1]. They have been widely used in mechanical industries as actuating elements due to their relatively low price, ease of installation, simple construction and flexibility in sizes and stroke lengths. As the wave of industry 4.0 surges, more and more factories are aiming at a transition into ''unmanned factories''. This new trend poses stricter requirements on the reliability of the pneumatic cylinders, as they are asked to work 24 hours a day, for continuous production and profitability of the factories. As a consequence, modern pneumatic cylinders are typically designed with very high reliability and long lifetime requirements [2], [3]. In addition, severe competition in the market poses strict requirements on the development cycles of the cylinders. How to evaluate the reliability of the pneumatic cylinders in such a short development cycle, then, becomes an important but still open problem.

Life tests are indispensable in the design and development phase of pneumatic cylinders, to estimate the reliability of the pneumatic cylinders designed and verify that the reliability specifications are satisfied [4]. Conventional life tests are implemented under normal stress levels but take a long time to generate enough failure data for reliability assessment. Due to fierce competition from the market, the acceptable duration of life tests is restricted and insufficient for conventional life tests to generate the amount of failure data sufficient for an accurate reliability assessment. As an alternative, accelerated life tests (ALTs) use elevated stresses to accelerate the failure process and, make accurate reliability assessments in feasible amounts of time [5], [6].

ALTs are widely used in different areas [7]–[9], but rarely on pneumatic cylinders. Belforte *et al.* [10] used an ALT method for quickly comparing the reliability of seal prototypes of different geometries and materials. In [11], ALT was performed to shorten the testing time required for evaluating the reliability of pneumatic cylinders. Chen *et al.* [12]

identified wear and tear as significant stresses for the ALT of pneumatic cylinders, and carried out both ALT and conventional life tests on pneumatic cylinders. Yang *et al*. [13] and Chang *et al*. [14] estimated the reliability of pneumatic cylinders using accelerated degradation data. Ambu *et al*. [15] used wear measurements and life tests of pneumatic actuators for proposing various re-design solutions. Since the actuators are typical mechanical components, the failure mechanisms that affect them are fatigue, wear, corrosion [16]. Riddar and Rudolphi [17] identified possible degradation mechanisms of the surface of the cylinder and investigated the influence of contact load, temperature and particle contamination on the friction and wear mechanisms. Also, various researchers concluded that mechanical sealing rings are the main wear parts in pneumatic actuators. Raparelli *et al*. [18] did some researches to evaluate the friction force between the seal and cylinder under normal working conditions.

Most of ALT studies on pneumatic cylinders have been conducted at component level: only the weakest component in the cylinder (e.g., seal ring) is tested and the reliability of the cylinder is assumed to be determined by its weakest component [19], [20]. Further, the sample size in the existing ALTs is often limited, which impairs the accuracy of the reliability assessment. In this paper, we design a system-level ALT plan for pneumatic cylinders. Complete failure data with a large sample size are obtained and used to accurately assess the reliability. The original contributions of this paper include:

(1) A systematic analysis is performed to identify the main failure mechanisms and significant stresses for pneumatic cylinders.
(2) A system-level ALT of pneumatic cylinders is designed and implemented.
(3) Data analysis shows that the proposed ALT plan requires 38.77% of the testing efforts of other conventional life tests.

The rest of the paper is organized as follows. Section II presents a system-level failure mechanism analysis of the pneumatic cylinder for identifying the stresses significant for ALT. In Section III, the ALT is designed based on the analysis in Section II. Section IV presents the results of the ALT and uses them to evaluate the reliability under normal operation conditions. The paper is concluded with a discussion on future works in Section V.

II. STRUCTURAL AND FAILURE MECHANISM ANALYSIS OF THE PNEUMATIC CYLINDER

A flowchart of the steps for the analysis of the reliability of pneumatic cylinders based on ALT is given in Figure 1. Failure mechanism analysis is the first step, which aims at identifying the significant failure mechanisms and stresses to be included in the design of the ALT. Failure mechanisms are the physical and (or) chemical processes that cause failure of the component/system under analysis [21]. In this section, we conduct failure mechanism analysis for the pneumatic cylinders: the structural decomposition of the pneumatic cylinder is given in Sect. II-A; a Fault Tree Analysis (FTA) is conducted in Sect. II-B; finally, the failure mechanism analysis is done in Sect. II-C.

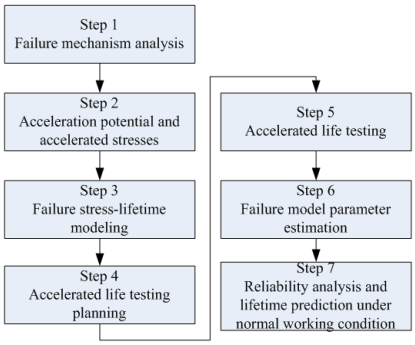

FIGURE 1. Flowchart of the steps for ALT-based reliability assessment of pneumatic cylinders.

A. STRUCTURE OF THE PNEUMATIC CYLINDER

The pneumatic cylinders considered in this study are space-saving thin cylinders whose axial and radial sizes are smaller than standard cylinders. They have a compact structure with strict restrictions on weight and space. The stroke is shorter than ordinary cylinders, and the sleeve and cover are made as a whole. The lid of the piston rod is fixed by a flexible retaining ring and the body of the cylinder is cuboid-shaped. This kind of cylinder is used to connect the fixtures and working pieces. A structural decomposition of the pneumatic cylinder is shown in Figure 2.

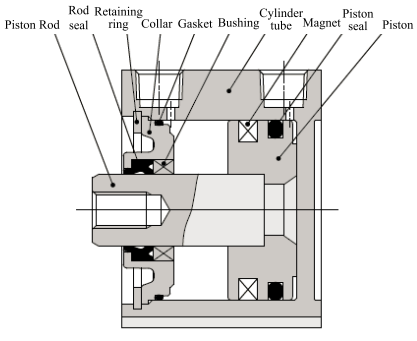

FIGURE 2. Structure of the pneumatic cylinder.

It can be seen from Figure 2 that the pneumatic cylinder consists of a cylinder tube in which a piston slides back and forward axially. Mounted on the piston is a piston seal, which slides against the inner surface of the cylinder tube. Rod seals made of Nitrile butadiene rubber (NBR) are fixed in the aluminum alloy casted collar. The cylinder is made of aluminum alloy and is anodized to increase its surface hardness. Typically, the cylinder tube and piston are made of aluminum and the piston seal and rod seal are made of NBR. The system is lubricated by grease before being assembled.

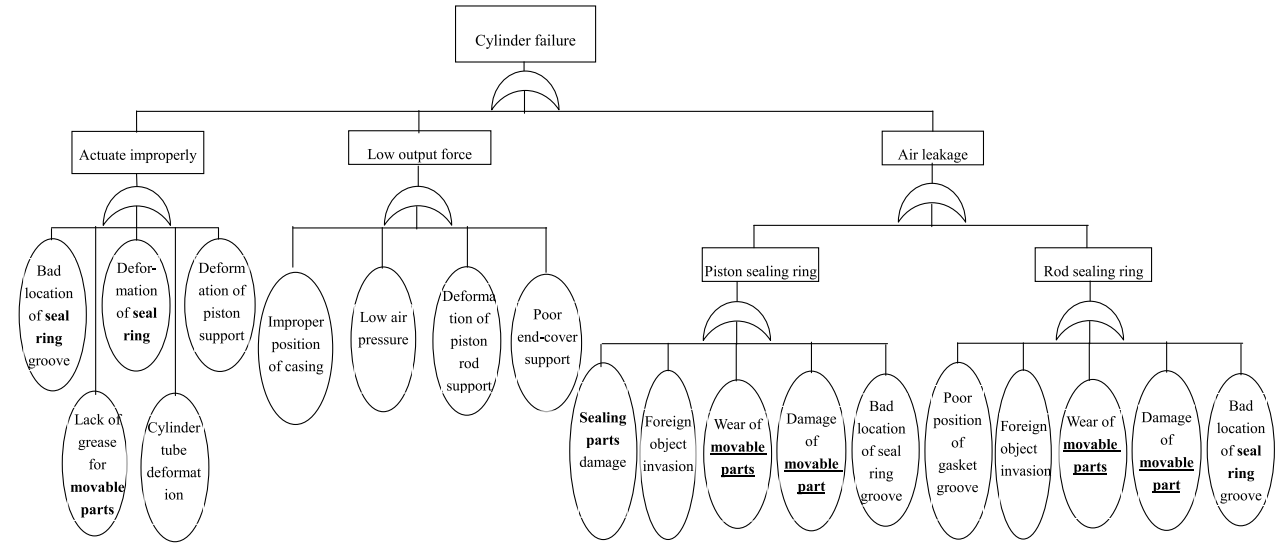

FIGURE 3. FTA of Cylinders.

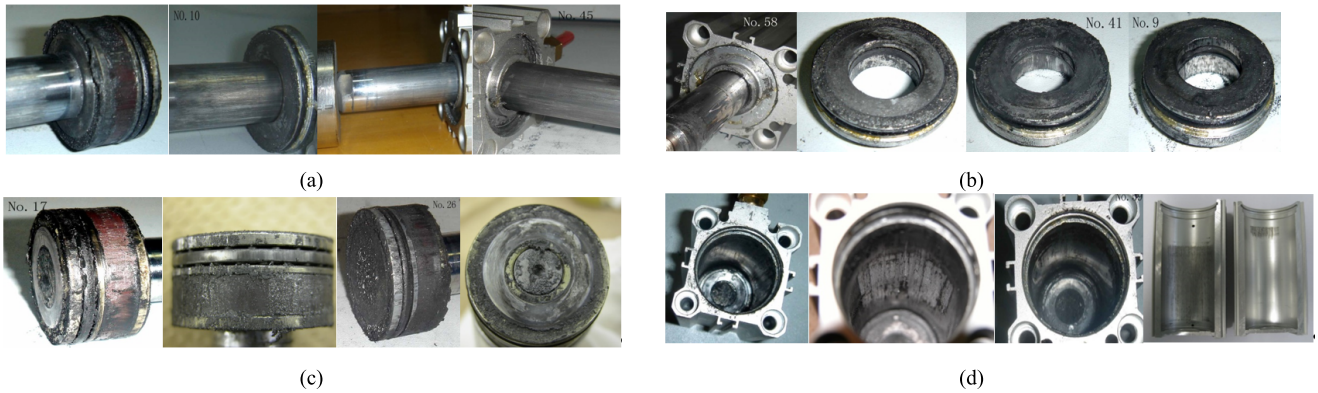

FIGURE 4. Observed field failures. (a) Piston rod scratch. (b) Parking seal wear. (c) Piston seal wear. (d) Cylinder tube debris.

B. FTA OF PNEUMATIC CYLINDER

FTA serves for laying down the logical relationships between system failure and component failure. The FTA of the tested cylinder is shown in Figure 3. It can be seen from the bold part of Figure 3 that there are three main failure modes: actuating improperly, low output force and air leakage. It can be concluded that the wear of the movable parts is the most critical failure mode. The two main moving parts of the cylinder are the piston and piston rod. The piston seal and piston rod seal are coated with grease. In the actuating process of the cylinder, the seals and the gaskets installed on the piston move back and forth, leading to repeated friction with the cylinder tube. The same phenomena occur in the piston rod, which produces repeated friction with the piston rod sealing ring mounted on the rod lid. Air leakage is observed normally in the two sealing rings, piston sealing ring and rod sealing ring.

Failed samples from field operations have been analyzed to verify the conclusions of the FTA. Typical field failures are shown in Figure 4. The observed failures verify the correctness and consistency of the FTA analysis: piston rod scratch is observed in Figure 4(a); parking seal wear is observed in Figure 4(b); piston seal wear is observed in Figure 4(c); piston tube debris is observed in Figure 4(d) [11].

During testing, the samples are loaded with the transverse load. Polarization is produced in the horizontal direction during the process of the movement. The wear of piston, piston rod and cylinder tube can be found more seriously on the load side, as compared to the other side.

Based on the FTA analysis and anatomy of the failed samples, it can be concluded that the main failure parts are the sealing rings, and the failure modes are wear and scratch on piston rod, parking seal, piston sealing ring and cylinder tube. The failure mechanisms leading to these failure modes are further analyzed in Sect. III-C.

C. FAILURE MECHANISM ANALYSIS

According to the analysis in Sect. II-B, the three main failure modes are improper actuation, low output force and

air leakage. For mechanical components, normally, possible failure reasons/mechanisms include fatigue, aging, wear and tear. The FTA analysis in Figure 3 identifies the piston parking seal ring as the weak component and its wear as the main failure reason. It is crucially necessary to analyze the failure mechanisms so that the stresses and acceleration potentials can be discovered. Figure 5 shows the failure mechanism caused by piston seal wear between inner tube wall surface and the seal surface [14]. Figure 6 shows the friction surface abrasion failure mechanism of the cylinder [22].

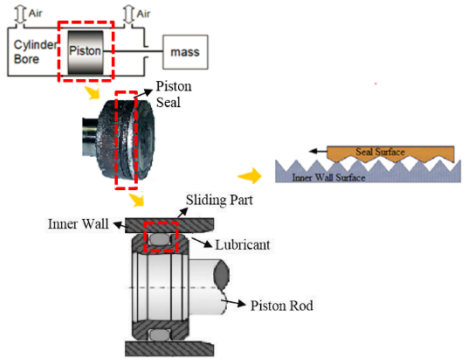

FIGURE 5. Pneumatic cylinder piston seal surface.

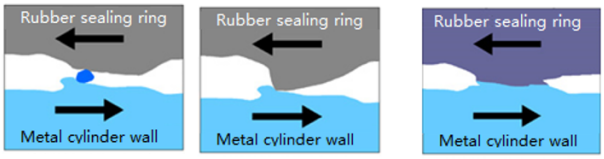

FIGURE 6. The friction surface abrasion failure mechanism of the piston cylinder (From left to right: three-body abrasion, two-body abrasion and adhesive abrasion).

As for pneumatic cylinders, in the first stage, due to the existence of the asperities between the contact surfaces (e.g. the aluminum alloy cylinder wall and rubber sealing ring), the wall would remove the material from the sealing ring. Therefore, two-body abrasive wear occurs. When the produced particles or debris are free to roll and slide over the contact surfaces, three-body abrasion occurs. Synergistic effects of high sliding frequency and heavy loads tend to produce higher temperature and result in thinner lubricant film, eventually causing the moving parts to contact directly [23]. This direct contact would create wear debris and material transfer, known as adhesive wear. Also, the high frequency of relative motion leads to surface fatigue, causing wear debris, superficial cracks and subsurface cracks. This aggravates the process of abrasive wear (two-body and three-body abrasive wear). In addition, as the temperature rises, oxidation wear occurs and dramatically accelerates the wear rate, making failure occur more easily, as shown in Figure 7 [24].

Besides, when the cylinder and the movable parts of the piston rod are damaged or lack grease, this is likely to cause slight deformation and adverse movement. Then, the cylinders would fail because of actuating improperly. The damage

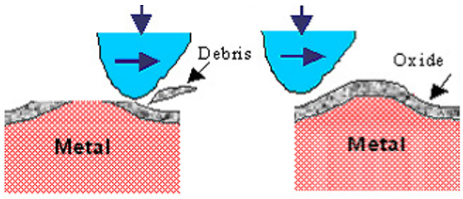

FIGURE 7. The oxidation wear failure mechanism of the piston cylinder.

of the movable parts of the piston rod easily causes the damage of the sealing rings and air leakage to occur, so the cylinders lose the ability to provide the required output force. In addition, the increased temperature contributes to the aging of the NBR piston seal and aggravates the wear to some extent.

Through the above analysis, it can be concluded that the main failure mechanism is the friction surface abrasion caused by wear of the piston seal ring. Once the friction surface abrasion goes beyond the threshold, the cylinder is judged to fail. In order to evaluate the reliability of cylinders, the ALT test is done at the system level. Since the quantities of wear and tear are hard to detect or observe in the test, we have to find some failure parameters which are easy to detect at the system level, and characterize the damage from wear and tear failure mechanism. These failure parameters are called failure criteria in this paper. There are some failure criteria that could be used, e.g., air leakage, minimum actuation pressure. Sometimes, functional failure may be visually inspected when the test samples lose the actuating function [11].

III. DESIGNING ALT TEST PLANS

A. IDENTIFYING TEST STRESSES

Based on the analysis of failure mechanisms in Section II, the main failure mechanisms are identified as wear and tear. Next, the significant stresses that affect the mechanisms need to be investigated, because ALT is designed to investigate the relationship between the lifetime characteristics and the stresses. The normal working conditions of the pneumatic cylinder can be represented by ambient temperature, working pressure and frequency. When the working fluid temperature inside the cylinder becomes too high or too low, abnormal abrasion of movable parts appears because of parking thermal expansion. Insufficient lubrication of movable parts aggravates their abrasion. If working air pressure and operating frequency increase, deformation of sealing-ring of cylinder, abrasion of movable pairs and air leakage will occur. When the cylinder actuating frequency increases, the reciprocating motion becomes faster, which causes the temperature to increase much more quickly. Then, lubrication deterioration and increasing abrasion of movable parts are caused. Table 1 reports how the three stresses, i.e., temperature, air pressure and frequency, affect the cylinder lifetime, and the related failure examples.

From the above analysis, the working stresses can be identified as working temperature, air pressure and

TABLE 1. Working stress effects on pneumatic cylinder life.

Working Stresses	Effect on products life	Examples of failures
Temperature	• Failure occurs suddenly in case of higher, lower temperature or thermal cycles. • Chemical reaction leads to the alternation of performance. • Material temperature characteristic parameters change. • Abrasion of movable parts increases because of seal expansion.	Lubricants evaporation, deterioration of lubricants and movable parts abrasion increases.
Pressure	• Failure is accelerated by the anti-friction of movable parts. • The accumulated fatigue and abrasion of reciprocating motion occurs.	O-shaped ring deformation, abrasion of movable parts (parking), air leakage increases.
Operating frequency	• Temperature rising between the contact surfaces caused by relative movements. • Accumulate abrasion and fatigue because of high operation frequency and velocity.	Lubricants deterioration and movable parts abrasion increases.

motion frequency. These stresses are candidates for accelerated stresses. Since air pressure is dependent on the compressor capability, it is not chosen as the acceleration stress. Meanwhile, load mass is fixed as constant during the testing. Therefore, only temperature and frequency are selected as the acceleration stresses used in ALT. In ALT, the temperature is designed to vary from 45°C to 75°C gradually, and the actuating frequency varies from 50 (cpm) to 125 (cpm) incrementally.

B. DETERMINING THE STRESS LEVELS AND SAMPLE SIZES

As shown in Sect. III-A, two stresses are used in the ALT: temperature and frequency. A full factor design on both temperature and frequency, with four levels each, is conducted. The temperature is increased by 10° for each level and the frequency is increased by 25 cycles per minute (cpm).

In terms of accuracy of reliability estimation, the sample size at each stress level should be as large as possible. In practice, a trade-off needs to be made between the estimation accuracy and the cost of the test. In this paper, considering the limitation on the cost of the test, the sample size at each level is set to be five units, except the groups 3, 4 and 8. For these groups, more samples (10) are tested because a pre-test shows larger variability in the data. A summary of the sample sizes of the ALT is given in Table 2.

TABLE 2. Sample sizes of the ALT.

Frequency	Temperature			
	45 C°	55 C°	65 C°	75 C°
50 CPM	$t_1^{(j)}$ (5)	$t_2^{(j)}$ (5)	$t_3^{(j)}$ (10)	$t_4^{(j)}$ (10)
75 CPM	$t_5^{(j)}$ (5)	$t_6^{(j)}$ (5)	$t_7^{(j)}$ (5)	$t_8^{(j)}$ (10)
100 CPM	$t_9^{(j)}$ (5)	$t_{10}^{(j)}$ (5)	$t_{11}^{(j)}$ (5)	$t_{12}^{(j)}$ (5)
125 CPM	$t_{13}^{(j)}$ (5)	$t_{14}^{(j)}$ (5)	$t_{15}^{(j)}$ (5)	$t_{16}^{(j)}$ (5)

C. EXPERIMENTAL SETTING

Movement of the cylinder is controlled by a valve according to the signals in Figure 8. A detailed presentation of the control signals can be found in Table 3, where in stage ①, the switching time refers to cylinder switching time or solenoid valve control signal to "on"; in stage ②, the standby time refers to the time during which the piston rod keeps resting; and in stage ③, the set speed refers to the average stretching-out velocity of the cylinder rod.

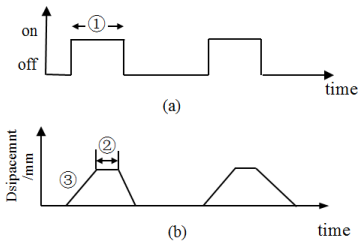

FIGURE 8. (a) Solenoid valve control signal. (b) Cylinder displacement waveform.

TABLE 3. The control signal.

Action frequency/ cpm	① Switch time /s	② Standby time/s	③ Set Speed(mm/s)	Maximum action per day/cycle
125	0.24	0.10	350	180000
100	0.30	0.10	250	144000
75	0.40	0.07	150	108000
50	0.60	0.10	100	72000

A test bench is designed for the ALT. The test circuit is shown in Figure 9, which includes a pressure source, the cylinder to be tested, a solenoid valve and an adjustable flow control valve acting as a speed controller. Switching of movement direction is controlled by a directional valve and the speed is adjusted by an adjustable flow control valve. The cylinders to be tested are installed horizontally and the load is applied to double acting cylinders.

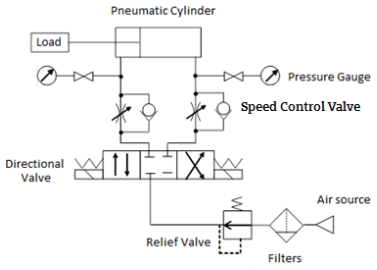

FIGURE 9. Test circuit for accelerated life test of pneumatic cylinders.

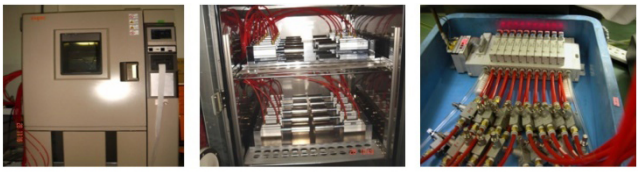

FIGURE 10. ALT test equipment. (a) Temperature chamber. (b) Samples mounted with load. (c) Control solenoid valve.

The test equipment is shown in Figure 10. A temperature chamber is used to accommodate the samples mounted with load and to maintain the temperature to a certain level. The solenoid control valve generates the control signal. For comparative analyses, another group of samples are tested at normal operation conditions, as shown in Figure 11.

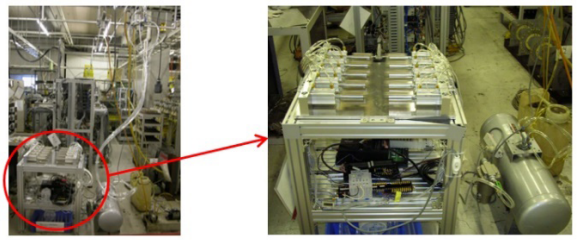

FIGURE 11. Normal life test equipment. (a) Test bench of conventional life testing. (b) Samples for conventional life testing.

D. END OF TESTING

According to the analysis in Sect. II-D, the pneumatic cylinder fails when one of the three events occur: air leakage exceeds the threshold value (including internal and external leakage); minimum working pressure exceeds the threshold value, functional failure occurs. The threshold values are determined according to ISO19973-2:

- Internal leakage: $5\text{cm}^3/\text{min}$
- External leakage: $10\text{cm}^3/\text{min}$
- Minimum actuating pressure: 0.12 MPa.

Functional failure such as stuck or unable to act is observed by visual inspections at pre-defined test intervals. The ALT terminates when all the test samples fail.

IV. RESULTS AND DISCUSSIONS

In this section, we present the data obtained from the ALT and use the data to estimate the reliability of the pneumatic cylinder at normal operation conditions. In Sect. IV-A, the appropriate ALT model for the pneumatic actuator is determined based on an initial analysis of the ALT data. The parameters of the ALT model are, then, estimated based on the ALT data in Sect. IV-B. In Sect. IV-C, the estimated parameters are used to estimate the reliability at normal operation conditions. In Sect. IV-D, the accuracy of the reliability estimation is validated using constant-stress life test data. Finally, in Sect IV-E, the ALT test plan is compared to the conventional constant-stress life test in order to demonstrate the advantages of the ALT.

A. ALT MODEL SELECTION

In this ALT, all the 95 test samples under the 16 stress levels are tested until failure. Therefore, 95 Time to Failure (TTF) data are obtained, as shown in Figure 12.

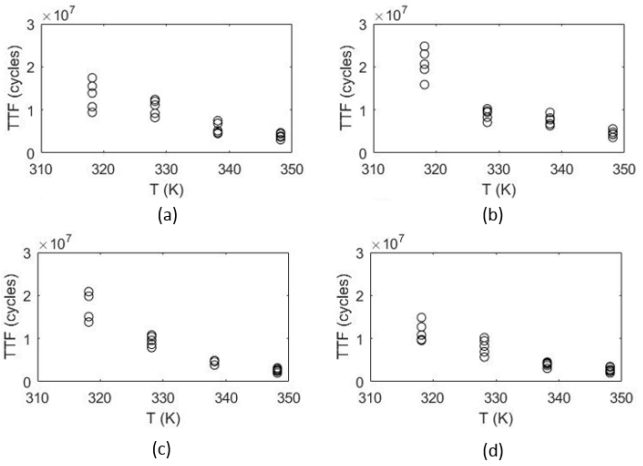

FIGURE 12. TTF data from the ALT. (a) $V = 50$ (cpm). (b) $V = 75$ (cpm). (c) $V = 100$ (cpm). (d) $V = 125$ (cpm).

ALT models encode knowledge on how the TTF distribution varies with stress levels. Typically, an ALT model includes two elements, *i.e.*, the probability distributions for the TTFs and the life-stress relation model that relates the life characteristics to the stress levels [25]. In the following subsections, we determine the TTF distribution and the life-stress relation model that most fit the ALT data.

1) TTF DISTRIBUTION

In ALT, the TTFs at different stress levels are often assumed to follow a common distribution [25]. In this paper, we consider four commonly used lifetime distributions, *i.e.*, exponential distribution, Normal distribution, Lognormal distribution, Weibull distribution, as candidate TTF distributions for the ALT data. An initial analysis is done by using probability plots to examine the fitness of each distribution to the ALT data, as shown in Figure 13- Figure 16 [25]. It can be seen from the Figures that the exponential probability plots significantly deviate from straight lines, indicating that the TTF data are unlikely to come from exponential distributions. The other three probability plots, on the other hand, exhibit straight-line

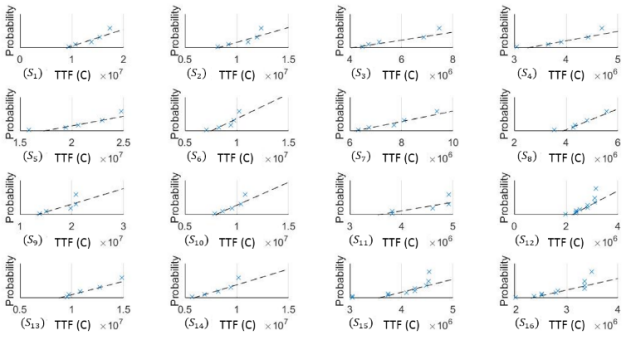

FIGURE 13. Exponential probability plots for the ALT data (C: cycles).

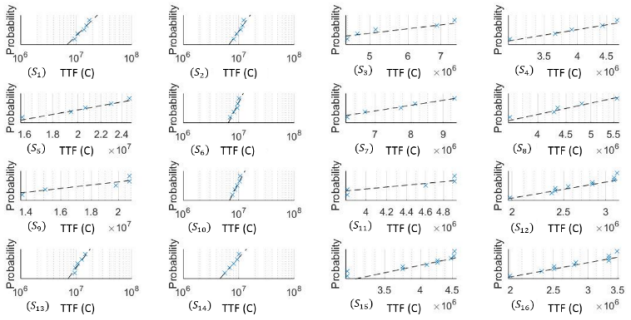

FIGURE 14. Lognormal probability plots for the ALT data (C: cycles).

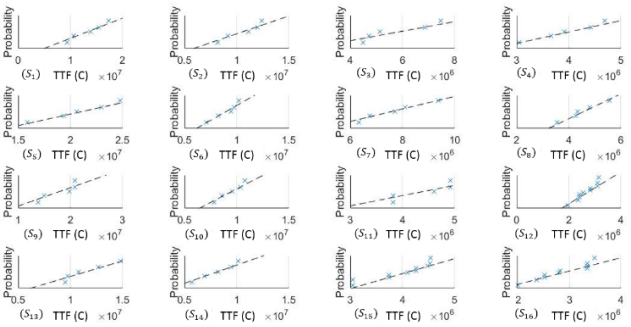

FIGURE 15. Normal probability plots for the ALT data (C: cycles).

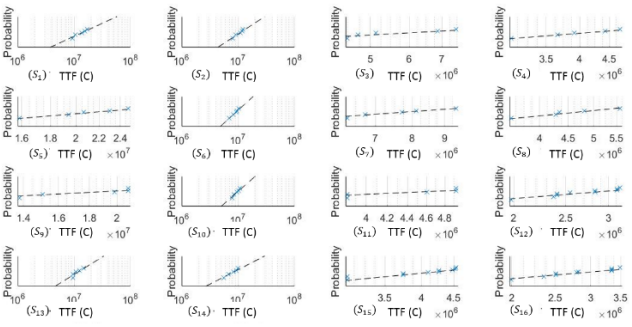

FIGURE 16. Weibull probability plots for the ALT data (C: cycles).

behaviors. Hence, Lognormal, Normal and Weibull distributions are all retained as possible TTF distributions to describe the ALT data.

Anderson-Darling tests are used to quantitatively examine the suitability of the distributions. The procedures of the test are summarized in Appendix A. The p values of the tests are given in Table 4. As shown in Table 4, under significance level $\alpha = 0.05$, we can reject the null assumption that the data come from an exponential distribution, while there is no strong evidence to reject Lognormal, Normal or Weibull distributions.

TABLE 4. p values for the anderson-darling tests.

		Weibull	Normal	Log Normal	Exponential
Stress levels	1	0.8224	0.8433	0.7658	0.0275
	2	0.4989	0.5333	0.4688	0.0140
	3	0.2590	0.2556	0.3141	0.0213
	4	0.9078	0.9289	0.8633	0.0133
	5	0.9613	0.9546	0.8624	0.0134
	6	0.6846	0.5977	0.4794	0.0108
	7	0.7940	0.8653	0.9100	0.0123
	8	0.7532	0.8172	0.8463	0.0128
	9	0.0781	0.1134	0.1077	0.0147
	10	0.8000	0.8481	0.8184	0.0100
	11	0.0966	0.1063	0.0929	0.0091
	12	0.2534	0.3429	0.3293	0.0005
	13	0.4545	0.4583	0.5559	0.0157
	14	0.8759	0.9142	0.8427	0.0231
	15	0.1602	0.1064	0.0541	0.0005
	16	0.1631	0.2565	0.2884	0.0007

To further choose among the three distributions, first note that all the three distributions have the same number of parameters (two in this case). Hence, the distribution with maximal likelihood value is chosen as the most appropriate as it best explains the observation data from the ALT. The values of the log likelihood function of the three distributions are compared in Table 5, where the log likelihood values are calculated by first calculating the Maximum Likelihood Estimators (MLE) for the parameters of each distribution, and, then, evaluating the value of the log likelihood function at the MLE parameters values:

$$LogL_{\text{MLE}} = \sum_{i=1}^{n_{str}} \sum_{j=1}^{n_{S,i}} \ln\left(l\left(t_{i,j}|\hat{\boldsymbol{\theta}}_{\text{MLE}}\right)\right), \tag{1}$$

TABLE 5. Comparison on the values of the log likelihood functions

	Lognormal	Normal	Weibull
Log likelihood	-1445.2	-1443.8	-1441.1

where n_{str} is the number of stress levels and in this case $n_{str} = 16$; $n_{S,i}$ is the sample size at the stress level i; $l(\cdot)$ is the likelihood function of the assumed distribution; $t_{i,j}$ are the observed ALT data and $\hat{\boldsymbol{\theta}}_{\text{MLE}}$ is the MLE of the distribution parameters and is calculated by

$$\max_{\boldsymbol{\theta}} LogL = \sum_{i=1}^{n_{str}} \sum_{j=1}^{n_{S,i}} \ln\left(l\left(t_{i,j}|\hat{\boldsymbol{\theta}}\right)\right). \tag{2}$$

It can be seen from the Table that Weibull distribution best explains the ALT data, although the differences in the log likelihood values are small. Therefore, it is assumed that at each stress level, the ALT data follow Weibull distributions.

2) LIFE-STRESS RELATION MODEL

Let T_i represent the TTF at stress level i. Following the analysis in Sect. IV-A-1, we assume that

$$T_i \sim Weibull\,(m_i, \eta_i)\,, \quad i = 1, 2, \cdots, n_{str}, \tag{3}$$

where m_i and η_i are the shape and scale parameters at stress level i, respectively. Life-stress relation models relate the parameters m_i and η_i to the stresses. To find such a relationship, the MLEs and the 95% confidence intervals for m_i and η_i are calculated, as shown in Table 6 and Table 7 (see Appendix B for details of calculation).

TABLE 6. MLEs for m_i

		LOWER BOUND	$\hat{m}_i$	UPPER BOUND
STRESS LEVELS	1	2.5833	5.2532	10.6825
	2	3.8880	8.1423	17.0519
	3	2.6300	5.2350	10.4203
	4	4.0049	8.1529	16.5970
	5	3.9970	8.1054	16.4369
	6	4.8945	10.2782	21.5838
	7	3.8960	7.6059	14.8483
	8	3.7647	7.3435	14.3242
	9	3.5955	7.6990	16.4861
	10	5.0874	10.4109	21.3050
	11	5.2910	11.1064	23.3137
	12	5.1870	8.5627	14.1354
	13	3.0943	6.0077	11.6639
	14	2.8743	5.8929	12.0817
	15	5.8411	9.9167	16.8360
	16	4.2160	6.9842	11.5702

In most common life-stress relation models, it is assumed that the shape parameters of the Weibull distribution do not change with stresses. It can be seen from Table 6 that although large estimation uncertainty exists in the MLEs, the assumption of common shape parameters can be justified, as the 95% confidence intervals at different stress levels overlap with one another. To quantitatively examine the reasonability of the assumption that the shape parameters under different stress levels are equal, a likelihood ratio test is conducted [25]. In the likelihood ratio tests, the ALT data from each stress level are compared to the data from the stress level 9, which is the closest to the normal operation condition, under the null assumption that the two data sets are from two Weibull distributions with a common shape parameter. Detailed procedures of the likelihood ratio test can be found in Appendix C. The p values of the tests are summarized in Table 8. It can be seen from the Table that under the confidence level $\alpha = 0.05$, there is no enough evidence to reject the null assumptions that the Weibull distributions have common shape parameters.

TABLE 7. MLEs for η_i

		LOWER BOUND	$\hat{\eta}_i$	UPPER BOUND
STRESS LEVELS	1	1.2240×10^7	1.4597×10^7	1.7408×10^7
	2	1.0070×10^7	1.1277×10^7	1.2628×10^7
	3	5.2297×10^6	6.2460×10^6	7.4598×10^6
	4	3.7505×10^6	4.2006×10^6	4.7047×10^6
	5	1.9679×10^7	2.2054×10^7	2.4716×10^7
	6	8.6448×10^6	9.4536×10^6	1.0338×10^7
	7	7.2054×10^6	8.1421×10^6	9.2006×10^6
	8	4.2376×10^6	4.8091×10^6	5.4575×10^6
	9	1.7180×10^7	1.9360×10^7	2.1816×10^7
	10	9.1051×10^6	9.9506×10^6	1.0875×10^7
	11	4.2758×10^6	4.6461×10^6	5.0485×10^6
	12	2.6292×10^6	2.8378×10^6	3.0629×10^6
	13	1.0630×10^7	1.2413×10^7	1.4494×10^7
	14	7.4981×10^6	8.7705×10^6	1.0259×10^7
	15	3.9356×10^6	4.2017×10^6	4.4857×10^6
	16	2.7839×10^6	3.0571×10^6	3.3570×10^6

Therefore, in this paper, we assume that

$$m_1 = m_2 = \cdots = m_{16} = m. \tag{4}$$

The dependence of η on the stresses is investigated using scatter plots, as shown in Figure 17 and Figure 18. It can be seen from the Figures that $\ln\eta$ is a linear function of $\ln V$, and a linear function of $1/T$. Therefore, we assume the following model for life-stress relationship:

$$\eta = A \cdot V^{-B} \cdot e^{C/T}, \tag{5}$$

where A, B and C are three parameters that need to be estimated from data; V is the frequency (measured in cpm) and T is the temperature (measured in Kalvin). Equation (5) can be viewed as a combination of inverse power law model (for frequency) and Arrhenius model (for temperature).

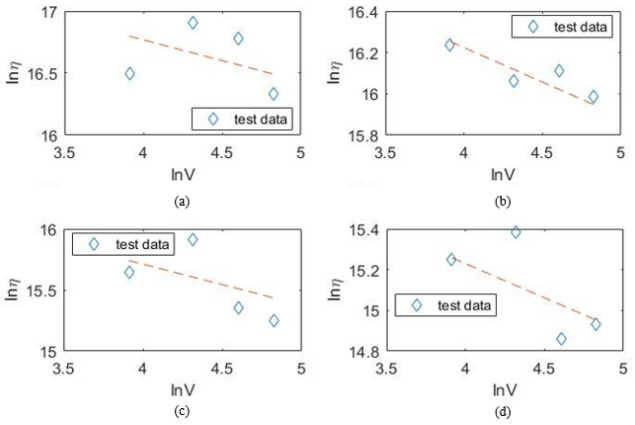

FIGURE 17. Dependence of η on V. (a) $T = 45$ (C°). (b) $T = 55$ (C°). (c) $T = 65$ (C°). (d) $T = 75$ (C°).

TABLE 8. *p* values for the likelihood ratio test.

STRESS LEVELS	1	2	3	4	5	6	7	8	9	10	11	12	13	14	15	16
p VALUES	0.4737	0.9177	0.4644	0.9141	0.9227	0.5954	0.9811	0.9269		0.5724	0.5005	0.8179	0.6315	0.6173	0.5883	0.8352

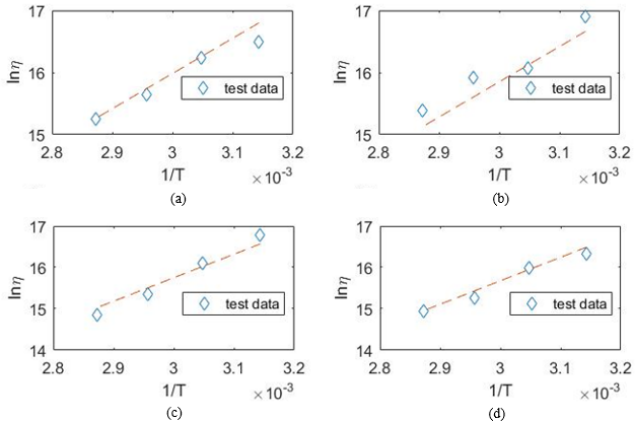

FIGURE 18. Dependence of η on T. (a) $V = 50$ (cpm). (b) $V = 75$ (cpm). (c) $V = 100$ (cpm). (d) $V = 125$ (cpm).

B. PARAMETER ESTIMATION

Equations (3)-(5) characterize the ALT model used in this paper. Maximum likelihood estimations are used to estimate the parameters from the ALT data. To achieve better estimation performances, let us first transform the parameters:

$$\beta_0 = \ln A, \quad \beta_1 = -B, \ \beta_2 = C, \ \beta_3 = \frac{1}{m}, \tag{6}$$

$$x_1 = \ln V, \quad x_2 = \frac{1}{T} \tag{7}$$

Then, at stress level i the distribution of the TTFs becomes

$$T_{i,j} \sim Weibull\left(\frac{1}{\beta_3}, \exp\left(\beta_0 + \beta_1 \cdot x_{1,i} + \beta_2 \cdot x_{2,i}\right)\right). \tag{8}$$

The likelihood function of the observed ALT data is given by

$$L = \prod_{i=1}^{n_{str}} \prod_{j=1}^{n_{S,i}} \frac{1}{\beta_3 \exp\left(\beta_0 + \beta_1 \cdot x_{1,i} + \beta_2 \cdot x_{2,i}\right)} \cdot \left(\frac{t_{i,j}}{\exp\left(\beta_0 + \beta_1 \cdot x_{1,i} + \beta_2 \cdot x_{2,i}\right)}\right)^{\left(\frac{1}{\beta_3}-1\right)} \cdot \exp\left(-\left(\frac{t_{i,j}}{\exp\left(\beta_0 + \beta_1 \cdot x_{1,i} + \beta_2 \cdot x_{2,i}\right)}\right)^{\frac{1}{\beta_3}}\right). \tag{9}$$

The log likelihood function is

$$\log L = \sum_{i=1}^{n_{str}} \left(- n_{S,i} \left(\ln \beta_3 + \frac{1}{\beta_3} \left(\beta_0 + \beta_1 \cdot x_{1,i} + \beta_2 \cdot x_{2,i}\right)\right) + \left(\frac{1}{\beta_3} - 1\right) \sum_{j=1}^{n_{S,i}} \ln t_{i,j} - \sum_{j=1}^{n_{S,i}} \left(\frac{t_{i,j}}{\exp(\beta_0 + \beta_1 \cdot x_{1,i} + \beta_2 \cdot x_{2,i})}\right)^{\frac{1}{\beta_3}} \right). \tag{10}$$

The MLEs $\widehat{\beta_0}$, $\widehat{\beta_1}$, $\widehat{\beta_2}$ and $\widehat{\beta_3}$ are calculated by maximizing the log likelihood function in (10). In this paper, we use the nonlinear optimization toolbox in Matlab 2016a for solving this optimization problem. The MLEs for the model parameters, can, then, be derived by taking a simple transformation:

$$\hat{A} = \exp\left(\widehat{\beta_0}\right), \quad \hat{B} = -\widehat{\beta_1}, \ \hat{C} = \hat{C}, \ \hat{m} = \frac{1}{\widehat{\beta_3}}. \tag{11}$$

Let $\widehat{\boldsymbol{\Sigma}}$ denote the observed covariance matrix, which is the inverse of the observed Fisher information matrix:

$$\widehat{\boldsymbol{\Sigma}} = \begin{bmatrix} -\frac{\partial^2 L}{\partial \beta_0^2} & -\frac{\partial^2 L}{\partial \beta_0 \beta_1} & -\frac{\partial^2 L}{\partial \beta_0 \beta_2} & -\frac{\partial^2 L}{\partial \beta_0 \beta_3} \\ -\frac{\partial^2 L}{\partial \beta_1 \beta_0} & -\frac{\partial^2 L}{\partial \beta_1^2} & -\frac{\partial^2 L}{\partial \beta_1 \beta_2} & -\frac{\partial^2 L}{\partial \beta_1 \beta_3} \\ -\frac{\partial^2 L}{\partial \beta_2 \beta_0} & -\frac{\partial^2 L}{\partial \beta_2 \beta_1} & -\frac{\partial^2 L}{\partial \beta_2^2} & -\frac{\partial^2 L}{\partial \beta_2 \beta_3} \\ -\frac{\partial^2 L}{\partial \beta_3 \beta_0} & -\frac{\partial^2 L}{\partial \beta_3 \beta_1} & -\frac{\partial^2 L}{\partial \beta_3 \beta_2} & -\frac{\partial^2 L}{\partial \beta_3^2} \end{bmatrix}^{-1} = \begin{bmatrix} Var(\widehat{\beta_0}) & Cov(\widehat{\beta_0}, \widehat{\beta_1}) & Cov(\widehat{\beta_0}, \widehat{\beta_2}) & Cov(\widehat{\beta_0}, \widehat{\beta_3}) \\ Cov(\widehat{\beta_0}, \widehat{\beta_1}) & Var(\widehat{\beta_1}) & Cov(\widehat{\beta_1}, \widehat{\beta_2}) & Cov(\widehat{\beta_1}, \widehat{\beta_3}) \\ Cov(\widehat{\beta_0}, \widehat{\beta_2}) & Cov(\widehat{\beta_1}, \widehat{\beta_2}) & Var(\widehat{\beta_2}) & Cov(\widehat{\beta_2}, \widehat{\beta_3}) \\ Cov(\widehat{\beta_0}, \widehat{\beta_3}) & Cov(\widehat{\beta_1}, \widehat{\beta_3}) & Cov(\widehat{\beta_2}, \widehat{\beta_3}) & Var(\widehat{\beta_3}) \end{bmatrix} \tag{12}$$

where $Var(\cdot)$ and $Cov(\cdot, \cdot)$ are the variance and covariance of the estimators, respectively and the partial derivatives are evaluated at $\widehat{\beta_0}, \widehat{\beta_1}, \widehat{\beta_2}, \widehat{\beta_3}$. The confidence intervals for the MLEs can, then, be derived based on large sample normal approximations [25]:

$$\begin{aligned} [A_L, A_U] &= \exp\left(\widehat{\beta_0} \pm z_{(1-\frac{\alpha}{2})} \cdot \sqrt{Var\left(\widehat{\beta_0}\right)}\right), \\ [B_L, B_U] &= -\left(\widehat{\beta_1} \pm z_{(1-\frac{\alpha}{2})} \cdot \sqrt{Var\left(\widehat{\beta_1}\right)}\right), \\ [C_L, C_U] &= \widehat{\beta_2} \pm z_{(1-\frac{\alpha}{2})} \cdot \sqrt{Var\left(\widehat{\beta_2}\right)}, \end{aligned} \tag{13}$$

where $z_{1-\alpha/2}$ is the $(1-\alpha/2)$ percentile of a standard normal distribution and α is the confidence level. For the shape parameter m, as it takes positive value, it is common practice to use log transformation to obtain a confidence interval [25]:

$$[m_L, m_U] = \left[\frac{1}{\widehat{\beta_3}} \cdot \exp\left(-\frac{z_{1-\alpha/2}\sqrt{Var\left(\widehat{\beta_3}\right)}}{\widehat{\beta_3}}\right), \frac{1}{\widehat{\beta_3}} \cdot \exp\left(\frac{z_{1-\alpha/2}\sqrt{Var\left(\widehat{\beta_3}\right)}}{\widehat{\beta_3}}\right)\right]. \tag{14}$$

Following Eqs. (11), (13) and (14), the MLEs and confidence intervals with $\alpha = 0.05$ for the parameters are calculated and their values are given in Table 9.

TABLE 9. MLEs and confidence intervals for the model parameters.

	Lower limit	Point estimate	Upper limit
A	0.4486	1.9293	8.2974
B	0.2816	0.4495	0.6174
C	5.2933×10^3	5.7238×10^3	6.1543×10^3
m	3.8388	4.4643	5.1887

C. RELIABILITY PREDICTION

The estimated parameters are used to predict the reliability at normal operation conditions. At the normal operation conditions, we have $V_N = 100$ (cpm) and $T_N = 42$ (°C). Let $x_{1,N} = \ln V_N$ and $x_{2,N} = 1/T_N$. Then, from Eq. (8), the TTF at normal operation condition follows a Weibull distribution

$$T_N \sim Weibull\left(\widehat{m_N}, \widehat{\eta_N}\right), \quad \widehat{m_N} = \frac{1}{\widehat{\beta_3}}, \widehat{\eta_N} = \exp\left(\widehat{\beta_0} + \widehat{\beta_1}\cdot x_{1,N} + \widehat{\beta_2}\cdot x_{2,N}\right). \tag{15}$$

It is easy to verify from Eq. (15) that $\ln T_N$ follows a Smallest Extreme Value (SEV) distribution with parameters

$$\mu_N = \frac{1}{\widehat{m_N}} = \widehat{\beta_3}, \quad \sigma_N = \ln\widehat{\eta_N} = \widehat{\beta_0} + \widehat{\beta_1}\cdot x_{1,N} + \widehat{\beta_2}\cdot x_{2,N}. \tag{16}$$

The variance-covariance matrix of μ_N and σ_N can be derived by

$$\widehat{\mathbf{\Sigma}_N} = \begin{bmatrix} Var(\mu_N) & Cov(\mu_N,\sigma_N) \\ Cov(\mu_N,\sigma_N) & Var(\sigma_N) \end{bmatrix} = \begin{bmatrix} \frac{\partial\mu_N}{\partial\beta_0} & \frac{\partial\mu_N}{\partial\beta_1} & \frac{\partial\mu_N}{\partial\beta_2} & \frac{\partial\mu_N}{\partial\beta_3} \\ \frac{\partial\sigma_N}{\partial\beta_0} & \frac{\partial\sigma_N}{\partial\beta_1} & \frac{\partial\sigma_N}{\partial\beta_2} & \frac{\partial\sigma_N}{\partial\beta_3} \end{bmatrix} \cdot \widehat{\mathbf{\Sigma}} \cdot \begin{bmatrix} \frac{\partial\mu_N}{\partial\beta_0} & \frac{\partial\mu_N}{\partial\beta_1} & \frac{\partial\mu_N}{\partial\beta_2} & \frac{\partial\mu_N}{\partial\beta_3} \\ \frac{\partial\sigma_N}{\partial\beta_0} & \frac{\partial\sigma_N}{\partial\beta_1} & \frac{\partial\sigma_N}{\partial\beta_2} & \frac{\partial\sigma_N}{\partial\beta_3} \end{bmatrix}^T. \tag{17}$$

Then, the confidence interval of η_N can be determined based on the large sample approximation on $\ln\widehat{\eta_N}$ [25]:

$$\left[\eta_{N,L}, \eta_{N,U}\right] = \exp\left(\ln\widehat{\eta_N} \pm z_{1-\frac{\alpha}{2}}\sqrt{Var(\sigma_N)}\right), \tag{18}$$

where $Var(\sigma_N)$ is determined by Eq. (17). The confidence interval of m_N can be calculated by Eq. (14). The predicted model parameters and the associated confidence intervals ($\alpha = 0.05$) are summarized in Table 10.

TABLE 10. Predicted model parameter at normal operation conditions.

	Lower limit	Point estimate	Upper limit
m_N	3.8388	4.4643	5.1887
η_N	1.7133×10^7	1.8799×10^7	2.0626×10^7

Percentile life t_p is a widely used reliability index. Suppose a given failure probability p is considered. The percentile life associated with p is defined as

$$t_p \triangleq \arg_t\left(R(t) = 1 - P_f\right). \tag{19}$$

Commonly used percentile BX lives in reliability analysis include B1, B5, B10, B50, B75, B90 lives, which correspond to failure probability of 0.01, 0.05, 0.1, 0.5, 0.75 and 0.95, respectively.

The estimates and confidence intervals of the t_p s can be derived based on the predicted parameter values in Table 10. In practice, the t_ps are often estimated using the SEV distribution [25]:

$$\widehat{t_p} = \exp\left(\mu_N + \Phi^{-1}(p)\,\sigma_N\right) \tag{20}$$

where $\Phi^{-1}(\cdot)$ are the inverse cumulative distribution function of a standard SEV distribution SEV (0, 1) and μ_N and σ_N are determined by Eq. (16). The confidence interval with confidence level α can be derived based on the large sample approximation on $\ln\widehat{t_p}$[25]:

$$\left[t_{p,L}, t_{p,U}\right] = \left[\widehat{t_p}/w, \widehat{t_p}\cdot w\right], \tag{21}$$

where w is given by

$$w = \exp\left(\frac{z_{1-\frac{\alpha}{2}}\sqrt{Var\left(\widehat{t_p}\right)}}{\widehat{t_p}}\right),$$
$$Var\left(\widehat{t_p}\right) = \widehat{t_p}^2\left(Var(\mu_N) + 2\Phi^{-1}(p)Cov(\mu_N,\sigma_N) + \left(\Phi^{-1}(p)\right)^2 Var(\sigma_N)\right). \tag{22}$$

In Eq. (22), $Var(\mu_N)$, $Cov(\mu_N,\sigma_N)$ and $Var(\sigma_N)$ are calculated by Eq. (17).

The confidence intervals are used to quantify the uncertainty in the estimators. In practice, one-sided lower bounds are also important as they give a lower bound to the reliability. The one-sided lower bound for t_p can be derived in a similar way:

$$t_{p,LL} = \widehat{t_p}\cdot\exp\left(-\frac{z_{1-\alpha}\sqrt{Var\left(\widehat{t_p}\right)}}{\widehat{t_p}}\right). \tag{23}$$

The B1, B5, B10, B50, B75, B90 lives and their confidence intervals with $\alpha = 0.05$ at normal operation conditions are predicted using Eqs. (20)-(23), as represented in Table 11. The predicted values in Table 11 are values of the percentile lives estimated with maximized likelihood. The two-sided confidence interval quantifies the uncertainty in the predicted values due to insufficient sample size: it is believed that if we can repeat the test a large number of times, roughly $(1-\alpha)\times 100\%$ confidence intervals will cover the true (unknown) percentile lives. The one-sided lower bound provides an estimate of the lower limit of the percentile lives: if we can repeat the test a large number of times, roughly $(1-\alpha)\times 100\%$ one-sided lower bounds will be less than the true (unknown) percentile lives.

TABLE 11. Predicted percentile lives (in cycles).

	Predicted value	One-sided lower bound	Two-sided confidence interval	
			Lower limit	Upper limit
B1 life	0.6706×10^7	0.5665×10^7	0.5485×10^7	0.8199×10^7
B5 life	0.9663×10^6	0.8494×10^7	0.8286×10^7	1.1268×10^7
B10 life	1.1354×10^7	1.0141×10^7	0.9923×10^7	1.2990×10^7
B25 life	1.4220×10^7	1.2948×10^7	1.2718×10^7	1.5899×10^7
B50 life	1.7317×10^7	1.5965×10^7	1.5719×10^7	1.9077×10^7
B75 life	2.0226×10^7	1.8747×10^7	1.8477×10^7	2.2141×10^7
B90 life	2.2661×10^7	2.1022×10^7	2.0721×10^7	2.4783×10^7

D. MODEL VALIDATION

A life test under normal stress levels has been conducted to validate the developed ALT model. Eight samples are tested to failure under $V = 100$ (cpm) and T = 42°C. The failure data under normal stress levels are given in Figure 19, which also shows the empirical CDF of the TTF calculated based on the medium rank method using the test data [26]:

$$\widehat{F}(t_{N,i}) = \frac{i - 0.3}{N_N + 0.4}, \tag{24}$$

where $t_{N,i}, i = 1, 2, \cdots, N_N$ are failure data at normal stress levels and $t_{N,1} \le t_{N,2} \le \cdots \le t_{N,N_N}$; N_N is the number of failure data and in this case, $N_N = 8$. In Figure 19, we also present the predicted percentile lives and their confidence intervals in Table 11. It can be seen that all the test data are close to the predicted values. Besides, the test data lie within the corresponding confidence intervals. Therefore, the developed ALT model can reasonably approximate the true behavior of the actuator's life and reliability.

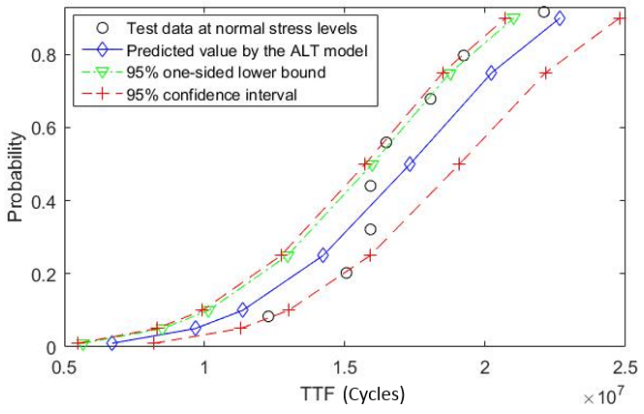

FIGURE 19. Failure data under normal stress levels.

A likelihood ratio test is used to quantitatively examine the reasonability of the developed ALT model. The null assumption of the test is H_0 : the TTF at normal stress levels has the same distribution as predicted by the ALT model. The alternate assumption is H_1 : the TTF at normal stress levels follow a different distribution. Under H_0, $t_{N,i}, i = 1, 2, \cdots, N_N$ are from *Weibull* $(\widehat{m_N}, \widehat{\eta_N})$, where $\widehat{m_N}$ and $\widehat{\mu_N}$ are given in Table 10. The likelihood L_0 can be calculated by [25]

$$L_0 = \prod_{i=1}^{N_N} \frac{\widehat{m}_N}{\widehat{\eta}_N} \cdot \left(\frac{t_{N,i}}{\widehat{\eta}_N}\right)^{\widehat{m}_N - 1} \cdot e^{-\left(\frac{t_{N,i}}{\widehat{\eta}_N}\right)^{\widehat{m}_N}}. \tag{25}$$

Under H_1, we further assume that the failure data come from a Weibull distribution with unknown parameters. MLE is used to estimate the parameters of the Weibull distribution. Then, the likelihood L_1 is calculated with the MLE of the model parameters. The test statistic T is calculated by

$$T = 2\left(\ln L_1 - \ln L_0\right). \tag{26}$$

The p value of the test is calculated by

$$p = \chi^2\left(T, K\right), \tag{27}$$

where the degree of freedom K equals the difference of unknown parameters in L_0 and L_1. In this case, we have $K = 2$. From Eqs. (26) and (27), the p value of the likelihood test is

$$p = 0.3279. \tag{28}$$

Therefore, it can be concluded that under a significance level $\alpha = 0.05$, the ALT model can accurately represent the true behavior of the actuator's life and reliability.

E. EFFECTIVENESS OF THE ALT PLAN

The ALT plan comprises of 16 stress levels and 95 test samples. The test time required by the ALT is

$$T_{ALT} = \sum_{i=1}^{n_{str}} \sum_{j=1}^{n_{S,i}} t_{i,j} = 7.3116 \times 10^8 \quad (cycles) \tag{29}$$

In this paper, we use the width of the 95% confidence interval of the estimated parameters to measure the precision of the test:

$$W = \frac{UL - LL}{\text{Point estimate}}, \tag{30}$$

where UL and LL are the upper and lower limits of the 95% confidence interval of the estimated parameter. From Table 10, the precisions of the estimated m and η at normal stress levels are calculated as

$$W_m = 30.24\%, \quad W_\eta = 18.58\%. \tag{31}$$

It can be seen that W_m is larger than W_η. Therefore, we use W_m to compare the performance of the ALT and the constant stress tests.

To achieve the sample amount of estimation precision, a large number of samples are needed in constant-stress life tests. Figure 20 investigates how the sample size and total test time (T_{Con}) change the precision of constant-stress life tests. The data in Figure 20 are obtained by generating n_{Con} failure

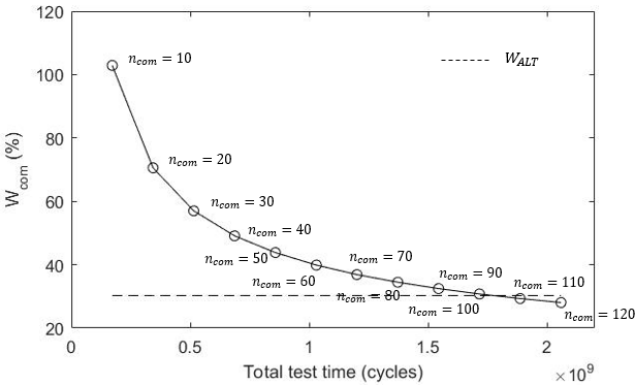

FIGURE 20. Precision of constant-stress life tests.

data from a known Weibull distribution with the parameters in Table 10 and estimate W_{Con} using Eqs. (21) and (30). The T_{Con} is calculated by summing all the n_{Con} failure data. For each value of n_{Con}, 10^4 simulations are performed and the 10^4 W_{Con} and T_{Con} are averaged to account for the uncertainty in the simulation.

It can be seen from the Figure that to achieve comparable precision to the ALT, the constant-stress life test requires at least 110 samples and the averaged total test time is 1.8859×10^9 (cycles). The ALT plan, on the other hand, requires only 7.3116×10^8 (cycles). Hence, adopting the ALT plan requires only

$$7.3116 \times 10^8 \Big/ 1.8859 \times 10^9 = 38.77\%$$

testing effort of the normal-stress life testing.

V. CONCLUSIONS

Pneumatic actuators are important mechanical components widely used in industries. As modern pneumatic cylinders are designed with high reliability requirements, how to estimate their reliability under strict time constraints remains a challenging task. In this paper, an ALT was designed and implemented to estimate the reliability of pneumatic actuators. The main failure mechanisms affecting the pneumatic actuators were identified as wears of the seal materials. By examining the failure mechanisms, the test stresses of the ALT were determined to be temperature and frequency. A full factor design was performed on both temperature and frequency, where each stress has four levels. A total number of 95 samples were tested at different stress levels until all test samples failed. The result of the test shows that

(1) when temperature is within 45° to 75° and the frequency is within 50 (cpm) to 125 (cpm), the TTF follow Weibull distributions with a common shape parameters, where the 95% confidence interval of the shape parameter is [3.8388, 5.1887] ;
(2) the dependency of the scale 1parameter on frequency can be described by an inverse power law model, while the dependency of the scale parameter on temperature can be described by an Arrhenius model.

The ALT data are used to predict the reliability of the actuator at normal operation conditions. Eight samples were tested until failure at normal stress levels to validate the developed ALT model. The results show that:

(1) under significance level $\alpha = 0.05$, the validation test data are described well by the same distribution as that predicted by the ALT model; therefore, the ALT model can accurately predict the reliability at normal operation conditions;
(2) to achieve the same estimation accuracy, the ALT requires only 38.77% of the testing time required by normal-stress life testing.

The original contribution of this work is the design and implementation of a system-level ALT on pneumatic cylinders. Important parameters like the shape parameters of the lifetime distributions are estimated from a large data set, which could be a valuable reference in designing future ALT plans. However, in this work, due to the limitation on testing equipment, we only consider temperature and frequency as test stresses in the ALT. Through the failure mechanism analysis, it is found out that apart from temperature and frequency, pressure is also a possible stress that could impact the reliability of the actuator. In the future, further ALT can be conducted to include pressure in the developed ALT model. Another interesting problem that deserves further investigation is to design accelerated qualification test plans for the actuator, where the calibrated ALT model in this paper can be used to design a qualification test plan under elevated stress levels, in order to reduce the time required for the qualification of the actuators.

APPENDIX

A. PROCEDURES FOR ANDERSON-DARLING TEST

The null assumption of an Anderson-Darling test is H_0 : the data follow the specified distribution. The alternate assumption is H_1 : the data do not follow the specified distribution. The test statistic used in the test is [27]:

$$AD = -n - \frac{1}{n}\sum_{i=1}^{n}(2i-1)\left(\ln F\left(X_i\right) + \ln\left(1 - F\left(X_{n-i+1}\right)\right)\right) \tag{32}$$

where n is the sample size, $F(\cdot)$ is the CDF of the specified distribution, and the samples X_i, $i = 1, 2, \cdots, n$ are sorted in ascending order. The procedures for Anderson-Darling test are summarized as follows:

Step 1: Estimate the unknown parameters in the specified distribution from the data;

Step 2: Calculate the test statistic AD using Eq. (32);

Step 3: Calculate the p value of the test. For most known distributions, critical values and their associated significance levels have been established in tables. The p values, can, then, be calculated by interpolate these tables.

Step 4: Draw conclusions by comparing the p value to the significance level.

B. MLEs FOR m_i AND η_i

As assumed in Eq. (3), T_i follows a Weibull distribution with parameters m_i and η_i. In practice, it is often derive the MLE of Weibull distributions by transforming them into SEV distributions. Let $\mu_i = 1/m_i$ and $\sigma_i = ln\eta_i$. Then, $\ln T_i \sim SEV(\mu_i, \sigma_i)$. The MLEs $\widehat{\mu}_i$ and $\widehat{\sigma}_i$ can be derived by maximizing the log likelihood function [25]:

$$\max_{\mu_i,\sigma_i} -n_{S,i}(\ln\mu+\sigma)+\left(\frac{1}{\sigma}-1\right)\sum_{j=1}^{n_{S,i}}\left(\ln t_{i,j}-\sigma\right) - \sum_{j=1}^{n_{S,i}}\left(\frac{t_{i,j}}{e^{\sigma}}\right)^{\frac{1}{\sigma}}. \quad (33)$$

Note that for sake of simplicity in presentation, we drop the index i in the subscripts in the rest of this section. Let the observed Fisher information matrix to be [25]

$$\hat{\boldsymbol{\Sigma}} = \begin{bmatrix} Var(\widehat{\mu}) & Cov(\widehat{\mu},\widehat{\sigma}) \\ Cov(\widehat{\mu},\widehat{\sigma}) & Var(\widehat{\sigma}) \end{bmatrix} = \begin{bmatrix} -\frac{\partial^2 L}{\partial\mu^2} & -\frac{\partial^2 L}{\partial\mu\partial\sigma} \\ -\frac{\partial^2 L}{\partial\mu\partial\sigma} & -\frac{\partial^2 L}{\partial\sigma^2} \end{bmatrix}^{-1} \quad (34)$$

where L is the likelihood function. The $100(1-\alpha)\%$ confidence interval of $\hat{\mu}$ can be derived based on large sample approximations on $\hat{\mu}$ [25]

$$[\mu_L, \mu_U] = \hat{\mu} \pm z_{1-\frac{\alpha}{2}}\sqrt{Var(\widehat{\mu})}. \quad (35)$$

The $100(1-\alpha)\%$ confidence interval of $\hat{\sigma}$ can be derived based on large sample approximations on $\ln\hat{\sigma}$ as σ always takes positive values [25]

$$[\sigma_L, \sigma_U] = \left[\hat{\sigma}/w,\ \hat{\sigma}\cdot w\right], \quad (36)$$

where w is given by

$$w = \exp\left(\frac{z_{1-\frac{\alpha}{2}}\sqrt{Var(\hat{\sigma})}}{\hat{\sigma}}\right). \quad (37)$$

The MLEs of m_i and η_i can be derived based on $\widehat{\mu}_i$ and $\widehat{\sigma}_i$:

$$\hat{m} = \frac{1}{\hat{\sigma}},\ \hat{\eta} = e^{\widehat{\mu}}. \quad (38)$$

The $100(1-\alpha)\%$ confidence intervals can also be derived:

$$[m_L, m_U] = \left[\frac{1}{\sigma_U}, \frac{1}{\sigma_L}\right], \quad [\eta_L, \eta_U] = \left[e^{\mu_L}, e^{\mu_U}\right]. \quad (39)$$

C. LIKELIHOOD RATIO TESTS FOR COMMON SHAPE PARAMETERS

A likelihood ratio test is used to test if data from two stress levels follow Weibull distributions with common shape parameters. The null assumption of the test is H_0 : the data from the two stress levels follow Weibull distributions with a common shape parameter m. The alternate assumption is H_1 : the data follow Weibull distributions with different shape parameters m_1 and m_2.

Let L_0 and L_1 represent the likelihood function under H_0 and H_1, respectively. The test statistic T is calculated by [25]

$$T = 2(\ln L_1 - \ln L_0). \quad (40)$$

It is known that T follows a χ^2 with K degrees of freedom, where K is the difference of unknown parameters in L_0 and L_1, and in this case, we have $K = 1$. The procedures of the likelihood ratio test can be summarized below:

Step 1: Calculate the MLE from data under H_0;

Step 2: Calculate the likelihood L_0 given the estimated MLE;

Step 3: Calculate the MLE from data under H_1;

Step 4: Calculate the likelihood L_1 given the estimated MLE;

Step 5: Calculate T using Eq. (40);

Step 6: Calculate the p value:

$$p = \chi^2(T, 1), \quad (41)$$

Step 7: Make decisions by comparing the p values to the significance level α.

ACKNOWLEDGMENT

The test data are from a cooperation project supported by SMC Technical center.

REFERENCES

[1] Z.-C. Qiu, B. Wang, X.-M. Zhang, and J.-D. Han, "Direct adaptive fuzzy control of a translating piezoelectric flexible manipulator driven by a pneumatic rodless cylinder," *Mech. Syst. Signal Process.*, vol. 36, no. 2, pp. 290–316, 2013.
[2] *Product Service Life at Festo*, Festo, Paris, France, 2013.
[3] *Pneumatic Fluid Power—General Rules and Safety Requirements for Systems and Their Components*, document DIN EN ISO 4414, 2011.
[4] E. A. Elsayed, *Reliability Engineering*, vol. 88. Hoboken, NJ, USA: Wiley, 2012.
[5] A. Angeli, B. Cornelis, and M. Troncossi, "Synthesis of sine-on-random vibration profiles for accelerated life tests based on fatigue damage spectrum equivalence," *Mech. Syst. Signal Process.*, vol. 103, pp. 340–351, Mar. 2018.
[6] W. B. Nelson, "A bibliography of accelerated test plans part II—References," *IEEE Trans. Rel.*, vol. 54, no. 3, pp. 370–373, Sep. 2005.
[7] L. Quagliato, D. Kim, N. Lee, S. Hwang, J. Domblesky, and N. Kim, "Run-out based crossed roller bearing life prediction by utilization of accelerated testing approach and FE numerical models," *Int. J. Mech. Sci.*, vol. 130, pp. 99–110, Sep. 2017.
[8] U. Proso, J. Slavič, and M. Boltežar, "Vibration-fatigue damage accumulation for structural dynamics with non-linearities," *Int. J. Mech. Sci.*, vol. 106, pp. 72–77, Feb. 2016.
[9] L. A. Escobar and W. Q. Meeker, "A review of accelerated test models," *Stat. Sci.*, vol. 21, no. 4, pp. 552–577, 2006.
[10] G. Belforte, L. Mazza, and C. Visconte, "Non contact wear measurement on pneumatic seals," *Tribol. Int.*, vol. 48, pp. 73–77, Apr. 2012.
[11] C. Juan, M. Jungong, and W. Qiang, "Fault mechanism analysis and accelerate life testing for pneumatic cylinders," in *Proc. 6th IEEE Int. Conf. Ind. Inform. (INDIN)*, Jul. 2008, pp. 1694–1699.
[12] J. Chen, Q. Wu, G. Bai, J. Ma, and Z. Wang, "Accelerated life testing design based on wear failure mechanism for pneumatic cylinders," in *Proc. 8th Int. Conf. Rel., Maintainability Saf. (ICRMS)*, Jul. 2009, pp. 1280–1285.
[13] Z. Yang, Y. X. Chen, Y. F. Li, E. Zio, and R. Kang, "Smart electricity meter reliability prediction based on accelerated degradation testing and modeling," *Int. J. Elect. Power Energy Syst.*, vol. 56, pp. 209–219, Mar. 2014.

[14] M. S. Chang, J. H. Shin, Y. I. Kwon, B. O. Choi, C. S. Lee, and B. S. Kang, "Reliability estimation of pneumatic cylinders using performance degradation data," *Int. J. Precis. Eng. Manuf.*, vol. 14, no. 12, pp. 2081–2086, 2013.
[15] R. Ambu, A. M. Bertetto, and L. Mazza, "Re-design of a guide bearing for pneumatic actuators and life tests comparison," *Tribol. Int.*, vol. 96, pp. 317–325, Apr. 2016.
[16] Z. Zeng, R. Kang, and Y. Chen, "Using PoF models to predict system reliability considering failure collaboration," *Chin. J. Aeronaut.*, vol. 29, no. 5, pp. 1294–1301, 2016.
[17] F. Riddar and K. Rudolphi, "Friction, wear and surface damage mechanisms of pneumatic clutch actuators," *Wear*, vol. 305, nos. 1–2, pp. 36–44, 2013.
[18] T. Raparelli, A. M. Bertetto, and L. Mazza, "Experimental and numerical study of friction in an elastomeric seal for pneumatic cylinders," *Tribol. Int.*, vol. 30, no. 7, pp. 547–552, 1997.
[19] G. Han and Y. Fu, "Tri-stress accelerated life test for cylinders," *Procedia Eng.*, vol. 16, pp. 554–563, 2011.
[20] B. S. Kang, J. H. Shin, and H. E. Kim, "A statistical analysis of elastomeric seal degradation in a pneumatic cylinder with variation of temperature," in *Proc. ASME/STLE Int. Joint Tribol. Conf.*, 2011, pp. 195–197.
[21] G. Belforte, M. Conte, and L. Mazza, "Low friction multi-lobed seal for pneumatic actuators," *Wear*, vol. 320, pp. 7–15, Dec. 2014.
[22] D. A. Rigney, L. H. Chen, M. G. S. Naylor, and A. R. Rosenfield, "Wear processes in sliding systems," *Wear*, vol. 100, nos. 1–3, pp. 195–219, 1984.
[23] Z. Zeng, Y. Chen, E. Zio, and R. Kang, "A compositional method to model dependent failure behavior based on PoF models," *Chin. J. Aeronaut.*, vol. 30, no. 5, pp. 1729–1739, 2017.
[24] B. Bhushan, *Handbook of Micro/Nano Tribology*. Boca Raton, FL, USA: CRC Press, 1998.
[25] W. Q. Meeker and L. A. Escobar, *Statistical Methods for Reliability Data*. Hoboken, NJ, USA: Wiley, 2014.
[26] N. R. Mann, R. E. Schafer, and N. D. Singpurwalla, *Methods for Statistical Analysis of Reliability and Life Data*. New York, NY, USA: Wiley, 1974.
[27] M. A. Stephens, "EDF statistics for goodness of fit and some comparisons," *J. Amer. Stat. Assoc.*, vol. 69, no. 347, pp. 730–737, 1974.

Authors' photographs and biographies not available at the time of publication.